Calculations of near-edge x-ray-absorption spectra of gas-phase and chemisorbed molecules by means of density-functional and transition-potential theory

L. Triguero and L. G. M. Pettersson
FYSIKUM, University of Stockholm, Box 6730, S-113 85 Stockholm, Sweden

H. Ågren
Institute of Physics and Measurement Technology, Linköping University, S-58183, Linköping, Sweden
(Received 14 July 1997; revised manuscript received 4 May 1998)

We explore the utility of density-functional theory (DFT) in conjunction with the transition-potential (TP) method to simulate x-ray-absorption spectra. Calculations on a set of small carbon-containing molecules and chemisorbed species show that this provides a viable option for obtaining excitation energies and oscillator strengths close to the experimental accuracy of core-valence transitions. Systematic variations in energy positions and intensities of the different spectra in the test series have been investigated, and comparison is made with respect to the static exchange-, self-consistent-field, and explicit electron-correlation methods. The choice between standard exchange-correlation functionals is shown to be of little consequence for the valence resonant, here π^*, parts of the x-ray-absorption spectra, while the long-range behavior of presently available functionals is found not to be completely satisfactory for Rydberg-like transitions. Implementing a basis set augmentation technique, one finds that DFT methods still account well for most of the salient features in the near-edge x-ray-absorption spectra, save for the multielectron transitions in the near continuum, and for some loss of Rydberg structure. For clusters modeling surface adsorbates, the DFT transition potential method reproduces well the spectral compression and intensity reduction for the valence level absorption compared to the free phase, provided fairly large clusters are taken into account. While for near-edge x-ray-absorption fine-structure (NEXAFS) spectra of free molecules the DFT-TP and Hartree-Fock/static exchange methods have complementary advantages, the DFT-TP method is clearly to be preferred when using clusters to simulate NEXAFS spectra of surface adsorbates. [S0163-1829(98)00136-2]

I. INTRODUCTION

X-ray spectroscopy has advanced a great deal owing to the intensity and high resolution obtainable with monochromatized synchrotron radiation. This has now provided x-ray spectra with a richness in structure that often matches low-energy spectra in the optical region. This, combined with the fact that x-ray spectroscopy, and in particular x-ray absorption near the edge, is a local probe technique, has created several entrances to electronic structure problems. These experimental advances have posed a continuous challenge to theory and calculations, and a variety of methods have been developed with different merits and limitations with respect to accuracy and size of the system, and with respect to the extension of the spectral interval under consideration.

The methods to simulate x-ray-absorption spectra (XAS) basically sort under the ''molecular orbital'' and the ''potential barrier'' interpretations. The latter, as manifested in the multiple scattering $X\alpha$ (MS$X\alpha$) method, has been extremely successful in the high-energy region, in particular in conjunction with extended x-ray-absorption fine-structure analysis, where it is used for structural investigations of ordered materials. Even in the low-energy region, below or close to the ionization edge, it seems that MS$X\alpha$ has provided the most popular simulation technique, as reflected by the extensive compilation in the book by Stöhr.[1] However, while this method fulfills the requirements of size and spectral interval quite well, it is more limited with respect to accuracy in the discrete part of the spectrum, probably owing to the muffin-tin implementation of the method, which often gives a poor representation of the true anisotropic molecular potential. Thus recent developments of the ''molecular-orbital'' branch of XAS simulations, in particular the so-called direct static exchange (STEX) technique that is scalable toward large species, have contested many of the assignments of the MS$X\alpha$ method in the discrete XAS region, even for quite simple systems like benzene and monosubstituted benzenes.[2,3] Of course, the STEX method, like other *ab initio* based techniques with orbital projections, has the comparative advantage of being systematically verifiable and of implementing rigorous criteria which in principle can be used to define ''good'' calculations. However, along with applications on many types of systems,[4] two practical limitations have been unraveled: the neglect of correlation in the reference states(s), and the neglect of interchannel interaction. Although the latter feature is possible to incorporate in principle, it is practically limited to small systems (see Ref. 5), as are the explicitly correlated molecular-orbital methods [multiconfiguration self-consistent field (MCSCF) and configuration interaction (CI)] and the propagator methods.

It seems relevant to attempt to improve the molecular potentials of the MS$X\alpha$ method[1,6] as well as another characteristic feature of that method, namely, the local-exchange approximation, by using modern density-functional methods that are orbital based and which utilize gradient-corrected exchange-correlation functionals. A third feature of the MS$X\alpha$ method, namely, the transition potential approximation, seems, on the other hand, to be well suited to carry over

and test in a density-functional theory (DFT) ''environment.'' Conceivably, such an attempt would also improve the problem of uncorrelated reference states in the *ab initio* molecular-orbital approaches, and perhaps also the problem of screening (using transition state potentials). The latter problem refers to two interrelated features that have become critical for the interpretation of near-edge x-ray-absorption fine structure (NEXAFS); the description of self-screening and the description of charge transfer.

Two recent works, by Stener, Lisini, and DeCleva[7] and Hu and Chong,[8] have already demonstrated the utility of the DFT transition potential (TP) for core-π^* valence excitations of some small molecules. Inspired by their success, here we make the extensions of considering NEXAFS *spectra*, that is all discrete transitions as well as an energy interval beyond the edge and of making applications to ''large systems,'' here clusters that model surface adsorbates. A third extension, namely, the exploration of the DFT-TP method in x-ray emission, which in many respects provides complementary information to NEXAFS, will be presented in a separate work.[9]

II. METHOD AND CALCULATIONS

The transition state method introduced by Slater[10,11] has been instrumental in calculations of spectra in the MS$X\alpha$ method as well as in many Hartree-Fock schemes. It includes a large part of the relaxation energy and is therefore particularly beneficial in cases where the estimate of the binding energy based on the frozen orbital approximation and Koopmans theorem

$$E_b(1s) = -\frac{\delta E_0(n_{1s})}{\delta n_{1s}} = -\epsilon_{1s} \tag{1}$$

fails. It can easily be shown that with a transition state with half an electron charge,

$$E_b(1s) = -\left.\frac{\delta E_0(n_{1s})}{\delta n_{1s}}\right|_{n_{1s}=1/2}, \tag{2}$$

the relaxation is included up to second order, which is sufficient for most core ionization/excitation problems.

We utilize the orbital-based density-functional theory as implemented in the DeMon program.[12] The method is rigorous only for the ground state, but it is a widely accepted praxis to use (or at least to explore the use of) orbital energies for excited states. With an orbital basis the Kohn-Sham equations take the forms

$$\hat{H}_{KS}\phi_i = \epsilon_i \phi_i, \tag{3}$$

$$\rho(\bar{r}) = \sum_{i}^{occ} \sum_{s}^{spin} n_{i,s} |\phi(\bar{r},s)|^2, \tag{4}$$

where $\hat{H}_{KS}$ is the operator with the exchange-correlation potential $V_{xc}[\rho(\bar{r})]$:

$$\hat{H}_{KS} = -\frac{1}{2}\nabla^2 - \sum_N \frac{Z_N}{|r_N - r|} + \int \frac{\rho(r')}{|r-r'|} dr' + V_{xc}[\rho(\bar{r})]. \tag{5}$$

Using density-functional theory, the variational principle can be applied to densities referring to any state with fractional occupancy. For example a ''ΔSCF'' Kohn-Sham theory is easily implemented using variational solutions from full and zero occupancies of the core orbital (SCF is self-consistent field):

$$IP_{1s} = E_{opt}|_{n_{1s}=0} - E_{opt}|_{n_{1s}=1}, \tag{6}$$

or, for the $1s$-π^* core excited state,

$$\Delta E_{1s,\pi^*} = E_{opt}|_{n_{1s}=0, n_{\pi^*}=1} - E_{opt}|_{n_{1s}=1, n_{\pi^*}=0}. \tag{7}$$

While this is both a convenient and accurate (see below) option for core ionized and first core excited states, it is not applicable for spectral calculations due to problems of nonorthogonality and collapse in optimizing higher excited states by separate state Kohn-Sham (KS)-SCF. An alternative way to obtain the spectrum is to diagonalize a potential constructed from orbitals where the ionized/excited electron has been removed. In doing so, one obtains the final state of the molecular excitation process described by the promotion of an electron from an occupied orbital to a virtual orbital that is an eigenvector of the KS operator. The excited electronic level is determined by the electrostatic field of the remaining molecular ion, which is frozen with respect to the interaction with the excited electron. The operator is obtained from the KS Hamiltonian [Eq. (5)] with spin orbital i unoccupied (unrestricted orbitals are assumed). The eigenvalues and eigenvectors describe the full spectrum of excitation energies and moments (the latter as dipole matrix elements over the ground-state orbital). This leads to nonorthogonal transition moments, and a potential that is quite attractive. Alternatively, one may use the transition potential formalism, in which the potential referring to one transition state gives the total spectrum and the full set of orthogonal eigenvectors. This leads to a less attractive potential with some advantages (as discussed below). The excitation energies are then simply expressed as $\Delta E_{exc} = \epsilon_f^T - \epsilon_{1s}^T$, i.e., as differences between transition potential orbital energies; ϵ_{1s}^T corresponds to the $1s$ ionization potential (IP), and ϵ_f^T to the term value for $1s$ excitation to level f. Due to the orthogonality the oscillator strengths then take the simple form of $\frac{2}{3}|\langle \phi_{1s}|\hat{r}|\phi_f\rangle|^2$. In the discrete part of the spectrum the eigenpairs of excitation energies and moments provide a true spectral representation, while in the continuum they may provide a primitive spectrum for a Stieltjes imaging procedure, in which a spectrum of order N is converted to a quadrature spectrum of order n ($n \ll N$) such that the first $2n$ spectral moments are reproduced. From the quadrature spectrum Stieltjes derivatives and the final Stieltjes-imaged photoionization cross sections are obtained in the continuum.[13]

The same double basis set technique as earlier implemented by Hartree-Fock-(STEX) (Ref. 14) is used in the DFT-TP procedure. A convenient option is to obtain bound molecular orbitals from a KS-SCF or a KS-TP optimization in a good molecular basis set and then to add a large diffuse basis set at the ionization site in the construction of the KS-TP potential matrix. The former is represented in these DFT calculations by the IGLO-III basis set of Ref. 15 both for

carbon and oxygen; it allows for an improved representation of the relaxation effects in the inner orbitals. For hydrogen the primitive $(5s)$ basis set from Ref. 16 was used, augmented with one p function and contracted to $[3s,1p]$. The diffuse basis set should be described by functions that are flexible for relaxation upon core excitation, and that, in the NEXAFS case, contain a large number of diffuse functions describing near-edge structures and the continuum. Such an augmented basis set technique improves the optimization timing considerably, but requires that possible redundancies in the final basis sets are checked for and removed. The large diffuse basis set contains typically over one hundred additional s, p, and d functions centered at the site of core excitation. In these calculations it corresponds to a $(19s,19p,19d)$ uncontracted diffuse basis set.

Several different functionals have been applied in the DFT-based calculations. The gradient corrections due to Perdew and Wang (PW86) (Ref. 17) and to Becke (B) (Ref. 18) for the exchange part, together with the Perdew[19] (P86) and the Perdew and Wang (PW91) (Refs. 20–22) for the correlation functional. The local-density-approximation (LDA) calculations are performed using the so-called VWN potential.[23]

For the smaller copper cluster models (up to Cu_{14}) the copper atoms were described at the all-electron level using the Wachters[24] basis set in an $[8s,5p,3d]$ contraction with one diffuse p and one d function added. The all-electron cluster description was used for all applications to hydrocarbon chemisorption, including the geometry optimization of acetylene and ethylene at the di-σ adsorption site in Cu(110), and for the optimization of CO on a Cu_{14} cluster modeling the on-top site in Cu(100). For the larger cluster models, e.g., Cu_{50} for CO/Cu(100) and Cu_{61} for N/Cu(100), the central Cu_5 subunit was described at the all-electron level, and the surrounding atoms described using a one-electron effective core-potential (ECP) model developed by Mattsson *et al.*[25] The core, including the $3d$ shell, is thus described by a static potential, which includes the effects of relaxation and polarization of the $3d$ orbitals, but which only treats the $4s$ (one-electron ECP) valence electrons explicitly.

III. RESULTS AND DISCUSSION

In the present work we make applications to NEXAFS spectra of carbonyl and hydrocarbon molecules, both free and chemisorbed on different copper substrates, and in addition study one example of a strongly interacting atomic adsorbate N/Cu(100). These compounds have been used as samples for high-resolution NEXAFS spectroscopy, and are also suitable for systematic studies by theory and computations. Their NEXAFS spectra show features that are characteristic also for many other unsaturated species, i.e., the strong discrete $1s\rightarrow\pi^*$ resonance, a weak remainder of a Rydberg progression converging to the ionization limit, a shape resonance in the σ channel above the ionization limit, and fine structures superimposed on the near-edge continuum. Having two localized core sites, carbon and oxygen, the carbonyls also display the role of local, atomic, selection rules for transition intensities that are characteristic for x-ray spectra of molecules.[26] Nitrogen in N/Cu(100) binds to the surface through a large N $2p$–Cu $3d$ interaction, which requires dynamical correlation to describe.[27,28]

Five series of calculations are presented and discussed; O $1s$ and C $1s$ spectra of carbonyl compounds; C $1s$ spectra of hydrocarbon compounds; NEXAFS spectra of clusters modeling CO adsorbed on the Cu(100) surface and acetylene and ethylene adsorbed on a di-σ site of the Cu(110) surface; and, finally, atomic nitrogen chemisorbed on Cu(100). The molecular compounds have been analyzed earlier with molecular-orbital SCF, STEX, and electron-correlation methods[29] and by MS$X\alpha$ calculations.[1] We pay special attention to the so-called static exchange technique, which is a fully *ab initio* technique, but at the same time extensive toward the full spectra and for large species, i.e., essentially the same ''coverage'' as the present DFT-TP method. We also remind the reader of the DFT calculations of XAS π^* transitions of molecular compounds by Stener, Lisini, and Decleva[7] and Hu and Chong.[8]

A. Molecular NEXAFS applications

The three carbonyl members investigated here, carbon monoxide (CO), formaldehyde (H_2CO), and acetone $[(CH_3)_2CO]$, have been prototypes for NEXAFS (Ref. 1) and electron-energy-loss spectroscopy[30] measurements. The latter simulate x-ray absorption at high electron impact energies and forward scattering. Like the C_2H_2 and C_2H_4 compounds included here, they are π-electron molecules for which the first XAS transitions have a strongly resonant character (π^* resonance), and collect much of the oscillator strengths of the discrete part. This peak is followed by the Rydberg-like transitions converging to the ionization edge.

1. Core to π^* transitions

In order to explore the accuracy of the DFT-TP approach, which has been used for the whole series of molecules and clusters in the present investigation, we first study the internal consistency of the results and then put them into context with other types of calculations for the $C_{1s}\rightarrow\pi^*$ and $O_{1s}\rightarrow\pi^*$ transitions. Table I collects results of excitation energies (eV) and oscillator strengths for these transitions from the DFT calculations using the $n_{1s}^{-1/2}$ transition potential (TP) and with different exchange-correlation potentials. The table indicates that the choice between the different, commonly used, functionals is not very decisive for the evaluation of the DFT-TP results, thus confirming the inherent consistency of the approach. They also confirm previous observations[7,8] of a very good experimental agreement for both transition energies and oscillator strengths for this transition.

The absolute transition energies as obtained from the $n_{1s}^{-1/2}$ transition potential are notoriously about 1.5–2 eV too large. The origin of this overestimate can be understood if the $\epsilon_{1s}(n_{1s}^{-1/2})$ energies are compared with the Kohn-Sham separate state energies for the $1s$ IP's and with experimental energies as listed in Tables II and III. The two latter values are in excellent agreement for the investigated cases; the overshooting of the $\epsilon_{1s}(n_{1s}^{-1/2})$ energies, and therefore also the transition $[\epsilon_{1s}(n_{1s}^{-1/2})-\epsilon_{\pi^*}(n_{1s}^{-1/2})]$ energies, can be assigned to higher-order contributions to the core relaxation energy not covered by $n_{1s}^{-1/2}$ transition-potential theory. A correction of the transition-potential NEXAFS energies

TABLE I. C_{1s} and O_{1s} excitation energies (eV) and oscillator strengths for a group of small molecules calculated in the DFT approach using the transition-potential (TP) method with different exchange-correlation potentials.

Molecules	PW86P86	$f(\times 10^{-2})$	BPW86	$f(\times 10^{-2})$	BPW91	$f(\times 10^{-2})$	Expt.	$f(\times 10^{-2})$
				Carbon in carbonyls				
CO	288.0	16.2	287.5	16.2	288.9	16.4	287.4[a]	15[b],16.7[c]
H_2CO	286.9	6.2	286.3	6.3	287.9	6.4	286.0[d]	6.6[d]
$(CH_3)_2C^*O$	287.6	3.3	287.1	3.3	288.4	3.3	287.1[e]	5.8[d]
				Oxygen in carbonyls				
CO	535.7	6.6	535.1	6.6	536.1	6.6	534.2[a]	5.4[f],5.6[b],6.0[d]
H_2CO	532.5	3.6	531.6	3.6	532.8	3.6	530.8[g]	3.25[f],7.2[b]
$(CH_3)_2CO$	532.8	3.0	531.9	3.1	533.0	3.0	531.3[g]	3.3[f],3.1[d]
				Carbon in hydrocarbons				
C_2H_2	287.8	8.5	287.1	8.7	287.9	8.9	285.9	-
C_2H_4	286.9	4.2	286.3	4.2	287.1	4.3	284.7	-

[a]From Ref. 52.
[b]From Ref. 53.
[c]From Ref. 54.
[d]From Ref. 55.
[e]From Ref. 56.
[f]From Ref. 57.
[g]From Ref. 30.

(ΔIP) as $[\epsilon_{1s}(n_{1s}^{-1/2}) - \Delta(\text{KS-SCF})] + \Delta E_{rel}$ therefore seems motivated, and also brings the energies into an excellent agreement with NEXAFS π^* excitation energies. The last correction term is for differential relativistic effects associated with the removal of one electron from the $1s$ orbital (carbon: 0.2 eV; nitrogen: 0.3 eV; oxygen: 0.4 eV). It is quite interesting to observe that, while in the HF-STEX approach corrections must be included for relativistic effects as well as

TABLE II. Excitation energies and ionization potentials for C($1s$) and O($1s$) x-ray absorption comparing the PW86P86 and BP86 functionals. Data in the two rightmost columns include the ΔIP correction (full potential relaxation and relativity; see text). All energies are in eV.

Molecule	V_{xc}	Exc. En.	ϵ_{1s}-IP	Δ(KS-SCF)	ΔIP	Corrected with ΔIP Exc. En.	IP
C*O	PW86P86	288.1	297.8	296.5	−1.1	287.0	296.7
	BP86	287.5	297.1	295.4	−1.5	286.0	295.6
H_2C^*O	PW86P86	286.9	296.2	294.7	−1.3	285.6	294.9
	BP86	286.3	295.5	294.1	−1.2	285.1	294.3
$(CH_3)_2C^*O$	PW86P86	287.6	295.4	293.8	−1.4	286.2	294.0
	BP86	287.0	295.6	-	-	-	-
C_2H_2	PW86P86	287.8	293.1	291.6	−1.3	286.5	291.8
	BP86	287.1	292.4	291.0	−1.2	285.9	291.2
C_2H_4	PW86P86	286.9	292.6	291.1	−1.3	285.6	291.3
	BP86	286.3	291.9	290.4	−1.3	285.0	290.6
C_2H_6	PW86P86	288.1	292.5	291.0	−1.3	286.8	291.2
	BP86	287.5	291.8	290.3	−1.3	286.2	290.5
CO*	PW86P86	535.7	544.5	542.8	−1.3	534.4	543.1
	BP86	535.1	543.5	541.9	−1.2	533.9	542.3
H_2CO^*	PW86P86	532.5	541.4	539.6	−1.4	531.1	540.0
	BP86	531.6	540.4	538.7	−1.3	530.3	539.1
$(CH_3)_2CO^*$	PW86P86	532.8	539.8	537.9	−1.5	531.3	538.3
	BP86	531.9	538.8	537.0	−1.4	530.5	537.4

TABLE III. DFT excitation energies and ionization potentials for C(1*s*) and O(1*s*) x-ray absorption obtained with the PW86P86 functional and compared to data obtained with the STEX technique (screened values) and with experiment. DFT data include the ΔIP correction (full potential relaxation and relativity, see text). All energies are in eV.

Molecule	Method	Exc. En.	IP
C*O	DFT	287.0	296.7
	STEX	289.1	297.3
	Expt.	287.4	296.2
H_2C^*O	DFT	285.6	294.9
	STEX	288.4	295.2
	Expt.	286.0	294.5
$(CH_3)_2\,C^*O$	DFT	286.2	294.0
	STEX	289.1	294.2
	Expt.	287.1	293.9
C_2H_2	DFT	286.5	291.8
	STEX	286.4	291.5
	Expt.	285.9	291.1
C_2H_4	DFT	285.6	291.3
	STEX	285.5	290.9
	Expt.	284.7	290.6
C_2H_6	DFT	286.8	291.2
	STEX	-	290.9
	Expt.	286.9	290.6
CO*	DFT	534.4	543.1
	STEX	534.5	541.3
	Expt.	534.2	542.6
H_2CO^*	DFT	531.1	540.0
	STEX	531.6	538.3
	Expt.	530.8	539.4
$(CH_3)_2CO^*$	DFT	531.3	538.3
	STEX	532.4	536.8
	Expt.	531.3	537.9

differential dynamical correlation (lowering the initial state) and additional relaxation effects from core basis set improvements (lowering final state),[31] in the DFT-TP approach, with the large core basis sets routinely applied, only the relativistic effects have to be added over the Δ(KS-SCF) correction; dynamical correlation effects seem adequately handled by the functionals applied.

As seen in Table II, the ΔIP correction is quite constant for C 1*s* and O 1*s* excitations and can thus easily be applied in the general case. We find this correction appropriate also for the larger clusters and actually also for the XES spectra of the considered molecules and clusters as well; see Ref. 9. The agreement with the π^* oscillator strengths is particularly rewarding; see further discussion below. The situation for the two conjugated molecules and the remaining carbonyls shows the same overall quality concerning IP's and excitation energies as the carbonyl compounds; see Tables II and III.

Tables IV and V display the role of the gradient corrections in the calculations of the C_{1s} and O_{1s} x-ray spectra using the DFT-TP potential for the CO molecule, and comparing with some other techniques. As seen in the tables, the form of the gradient correction is not significant, and the relative intensities and differences of transition energies are quite stable. A comparison with data obtained from other calculations is also given in Tables IV and V. LDA values included indicate that they are not of a quality usable for NEXAFS. Other previous calculations utilize methods as different as STEX, SCF/MCSCF/CI, and the ADC(2) propagator methods, and by their comparison we obtain frozen orbital, relaxation, screening relaxation, and correlation contributions to the spectra (more data from other methods can be found in Refs. 7 and 29). The Δ(KS-SCF) value is also stable and agrees quite well with the previous ΔSCF/ΔMCSCF results[29] (or even better). The IP's obtained from the core orbital energies of the $n_{1s}^{-1/2}$ transition potential are, however, quite dependent on the functional, and require correction for the XAS calculations as discussed above. It is of interest here to learn that the $n_{1s}^{-1/2}$ transition state potential not only includes relaxation (comparison with STEX data) but also overcomes some of the problems of the π^*-electron screening (comparison with ΔSCF data), and apparently reaches as far as the accuracy of electron-correlation data. A clearcut rationalization with respect to these *ab initio* results is, however, not possible; we see that the $X\alpha$ entry[32] is only a few percent from experiment, which might indicate that it is the TP rather than the DFT feature that makes the DFT-TP method successful here. With more variational freedom the unrestricted scheme of course allows additional stabilization of the transition energies over the calculations based on spin-restricted orbitals.

The sensitivity of the computed spectra to the form of the potential is illustrated in Fig. 1. The $n_{1s}^{-1/2}$ TP is motivated because it includes relaxation effects up to second order. The $N-1$ (bare core hole) potential gives substantially poorer results, artificially pushing the spectrum up by many eV. For such a potential, DFT is clearly inferior to the *ab initio* static exchange method. There is also a possibility to use fractional (half) occupancy of the excited valence level as well: $E_{exc} = \epsilon_{\pi^*}(n_{\pi^*}^{1/2}) - \epsilon_{1s}(n_{1s}^{-1/2})$; see first column entries of Tables IV and V. This leads to a lowering of the π^* excitation energy by roughly an eV (shown also in the context of MS$X\alpha$ in Ref. 1). It is, however, from both physical and technical reasons questionable to obtain higher states other than the first one in the NEXAFS spectrum with such a ''state-specific'' approach.

The experimental agreement for both oxygen and carbon transitions is also rewarding from the point of view of the completely different characters of the excitations. The extra relaxation of the bound electrons due to the presence of the excited orbital is very different in the two spectra. This difference can be rationalized by the localization of the π^* orbital; it is a carbonlike self-screening orbital that ''collapses'' onto the carbon core upon the $C_{1s} \rightarrow \pi^*$ core excitation. This induces a large oscillator strength, collecting most of the intensity from the remainder of the Rydberg progression. In the corresponding oxygen excitation the π^* level is antiscreening and retains (or even enhances) the carbon character, and the oxygen core hole is screened through the occupied orbitals. This screening is seemingly accounted for by the DFT-TP potential, and the presence of the π^* electron does not change the process to any significant extent. Much of these characteristics for free CO are main-

TABLE IV. Role of the gradient corrections in the calculations of the C_{1s}-π^* x-ray transition energies and oscillator strengths using transition potentials for the CO molecule. All energies are in eV.

Methods	DFT-TP[a]	$f(\times 10^{-2})$[b]	DFT-TP[c]	$\epsilon_{1s}^{-1/2}$(TP)-IP[d]	Δ(KS-SCF)[e]
LDA(IGLO)	284.3	16.7	285.5	293.9	292.7
LDA(DZP)	286.5	16.7	287.7	296.3	294.9
PW86P86	288.1	16.2	289.4	297.8	296.5
PW86PW91	289.4	16.4	290.8	299.6	296.2
BP86	287.5	16.2	288.9	297.1	295.4
BPW91	288.9	16.4	290.2	298.8	295.5
Other methods					
STEX[f]	289.1	13.0	-	-	-
ΔSCF[f]	288.3	15.5	-	-	297.3
ΔMCSCF[g]	288.7	14.0	-	-	-
ADC(2)[g]	287.5	14.2	-	-	-
$X\alpha$[h] (DZP)	291.5	14.1	-	-	300.2
Expt.	287.4,287.3	16.7,15.0	-	-	296.2

[a]DFT excitation energies (ϵ_{π^*}-ϵ_{1s}) with $n_{1s}^{-1/2}$ and $n_{\pi^*}^{1/2}$ transition state potentials.
[b]DFT oscillator strengths corresponding to A.
[c]DFT excitation energies (ϵ_{π^*}-ϵ_{1s}) with $n_{1s}^{-1/2}$ transition state potential.
[d]Ionization potential as ϵ_{1s} with $n_{1s}^{-1/2}$ transition state potential.
[e]Ionization potential KS Δ(SCF) computed from total energies as $E_T(n)-E_T(n^{-1})$.
[f]From Ref. 29.
[g]From Ref. 58.
[h]From Ref. 32.

TABLE V. Role of the gradient corrections in the calculations of the O_{1s}-π^* x-ray transition energies and oscillator strengths using transition potentials for the CO molecule. All energies are in eV.

Methods	DFT-TP[a]	$f(\times 10^{-2})$[b]	DFT-TP[c]	$\epsilon_{1s}^{-1/2}$(TP)-IP[d]	Δ(KS-SCF)[e]
LDA(IGLO)	530.3	6.8	531.1	538.9	537.7
LDA(DZP)	533.9	6.7	534.7	542.5	540.9
PW86P86	535.7	6.6	536.7	544.5	542.8
PW86PW91	536.9	6.4	537.9	546.1	542.5
BP86	535.1	6.6	535.8	543.5	541.9
BPW91	536.1	6.6	537.1	545.1	541.6
Other methods					
STEX[f]	534.5	5.3	-	-	-
ΔSCF[f]	535.0	5.7	-	-	541.5
ΔMCSCF[g]	536.43	6.17	-	-	-
ADC(2)[g]	532.9	7.1	-	-	-
$X\alpha$[g] (DZP)	541.0	6.1	-	-	548.6
Expt.	534.2	6.0,5.4	-	-	542.6

[a]DFT excitation energies (ϵ_{π^*}-ϵ_{1s}) with $n_{1s}^{-1/2}$ and $n_{\pi^*}^{1/2}$ transition state potentials.
[b]DFT oscillator strengths corresponding to A.
[c]DFT excitation energies (ϵ_{π^*}-ϵ_{1s}) with $n_{1s}^{-1/2}$ transition state potential.
[d]Ionization potential as ϵ_{1s} with $n_{1s}^{-1/2}$ transition state potential.
[e]Ionization potential KS Δ(SCF) computed from total energies as $E_T(n)-E_T(n^{-1})$.
[f]From Ref. 29.
[g]From Ref. 58.
[h]From Ref. 32.

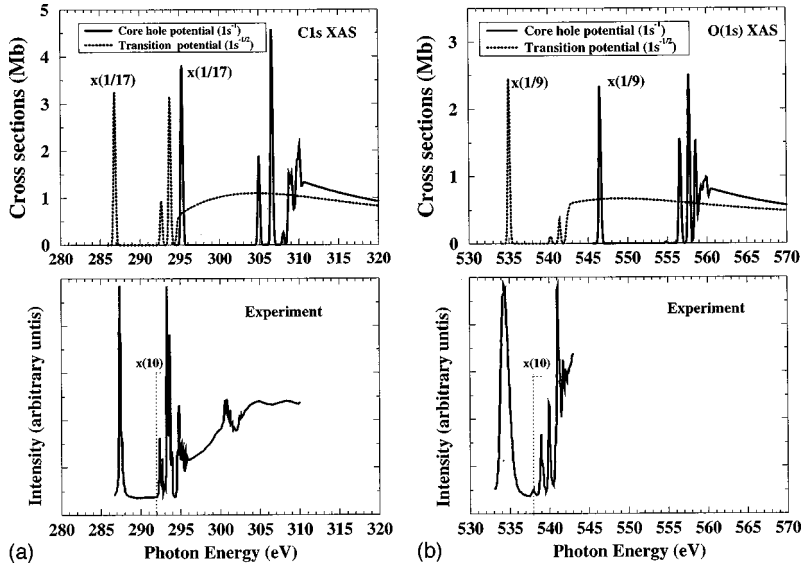

FIG. 1. Carbonyl C_{1s} and O_{1s} NEXAFS spectra of CO. (a) Calculations from the DFT-TP method with half-core orbital occupancy and from DFT-TP with a full core hole. The spectra are convoluted by a full width at half maximum (FWHM) of 0.3 eV. (b) Experimental spectra published in Ref. 59.

tained in different bonding environments.[29,33]

For H_2CO we find a good agreement between calculated π^* oscillator strengths and C 1*s* experimental values; the quite different experimental values for the oscillator strength of the O_{1s} excitation are possible to distinguish theoretically. One finds the same trend as for CO between the STEX, SCF, and MCSCF values on the one hand and the DFT values on the other. Corresponding energy data for the other molecules in the series are compiled in Tables II and III for two selected functionals (PW86P86, BP86). The gross picture remains the same; a fairly small dependence on functional, a close agreement between separate-state Kohn-Sham and experimental ionization potentials, and transition-potential orbital energies which are notoriously too large, by about 1.5 and 1.9 eV for carbon and oxygen 1*s* ionization, respectively. We thus find that the DFT approach predicts both $O_{1s} \rightarrow \pi^*$ and $C_{1s} \rightarrow \pi^*$ oscillator strengths sufficiently well to be used for a systematic analysis of the larger carbonyl compounds.

The larger carbonyl compounds show regular trends with increasing π^* energy, decreasing π^* intensity, and depletion of the Rydberg structure. Some of these changes can be ascribed to the dual effect of initial state population of the π^* orbital and of final-state delocalization of the same orbital.[29,34] As seen in Tables II and III the acetone $[(CH_3)_2CO]$ IP's are significantly decreased from their CO values. Comparatively, the methyl unit is more electronegative than the H atom, and exerts an inductive effect on the CO group with the net effect that the C 1*s* and O 1*s* IP's decrease. A covariation of the excitation energies takes place only for O 1*s*-π^* excitation while the C 1*s*-π^* excitation remains largely the same, which can be assigned the aforementioned self-screening of the π^* level in the carbon case, something that seems well reproduced by the DFT-TP theory.

2. Spectra of carbonyl molecules

Figure 2 collects the C and O *K*-edge NEXAFS spectra of carbonyl carbon and oxygen atoms. As seen in the figure the strong π^* resonance is followed by several peaks due to excitations to Rydberg orbitals. Some systematic trends can be discerned in the spectra. First, the intensity of the main peak is sharply decreased when the two unpaired bonds of the carbonyl become saturated. Since the carbonyl carbon is directly interacting with the H or the CH_3 groups, the carbon spectra are more influenced by the nature of the bonding groups than are the oxygen spectra. The spectra resulting from the carbonyl carbon 1*s* excitation are simpler than the O_{1s} excitation spectra when both unpaired bonds are saturated by the methyl groups. The experimental observation is unfortunately complicated by the overlap of two C_{1s} excitation series in the acetone case.

One observes a general enhancement of structure and intensity in the NEXAFS spectra going from CO to H_2CO, especially for the carbon spectrum, which now shows intensity for the upper discrete levels, in particular the $3p\sigma$ level at 292 eV, which must be assigned mixed Rydberg valence character. This enhancement is sufficiently strong to be of relevance also for the larger systems in the carbon case. The carbonyl oxygen seems to be less perturbed by the environment. The shape resonance behavior is also different, being stronger for the C 1*s* excitations. The different bonding has more significant influence on the structure of the Rydberg peaks.[29] Much of these characteristics are covered by the DFT-TP theory when implemented in the augmented basis set technique.

Formaldehyde provides a good test case in that the experimental C 1*s* spectrum shows several structures in the Rydberg region. These have successfully been assigned to molecular symmetry as well as to atomic subsymmetry contributions by means of the STEX technique using also quantum defect and Mulliken population analysis.[29] In the O 1*s* experimental spectrum of formaldehyde, only three Rydberg peaks were reported;[30] the two strong peaks are not resolved because of the limited resolution (0.5 eV).

The convolution gives indeed a three-Rydberg-peak structure [see Fig. 2(e)] quite similar to the experiment (Fig. 1 of

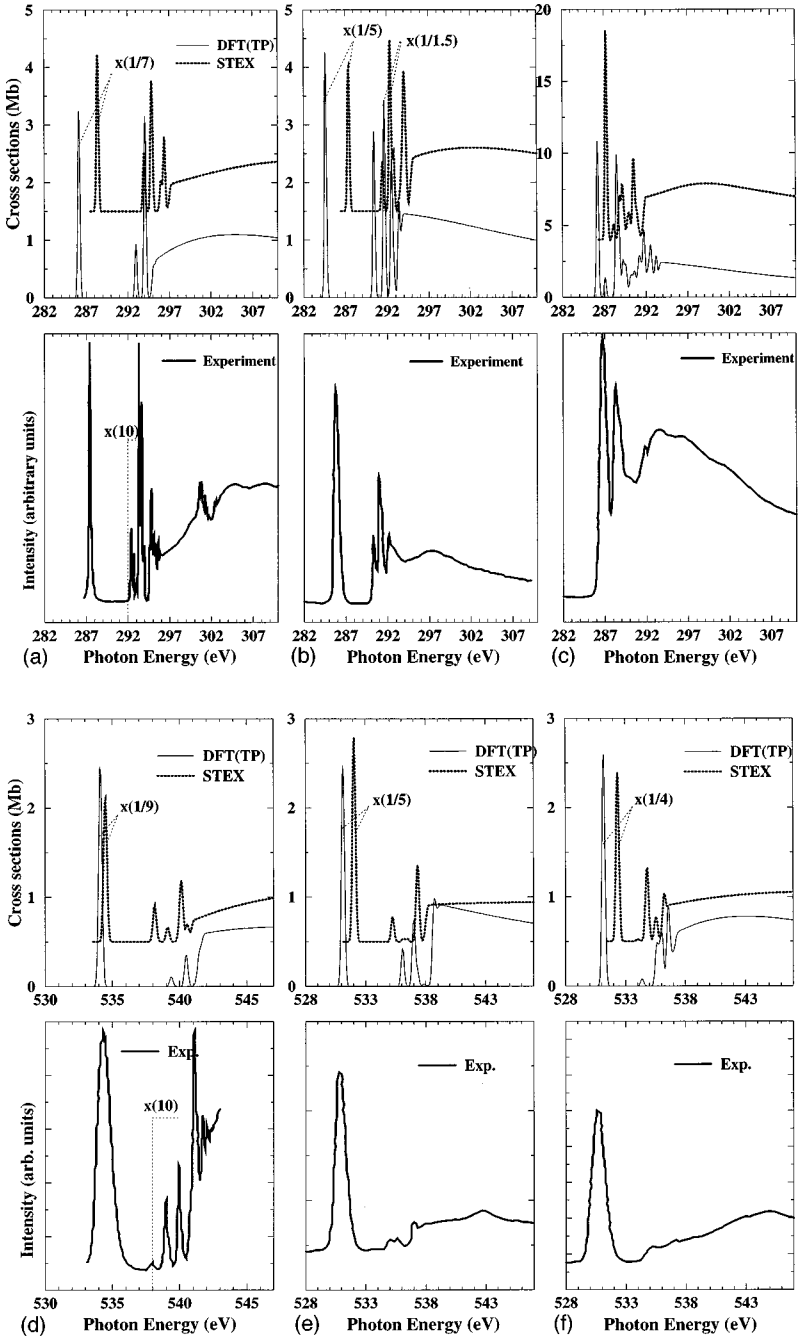

FIG. 2. C_{1s} and O_{1s} NEXAFS spectra of some carbonyl compounds (a) C 1*s* of CO. (b) C 1*s* of H_2CO; (c) C 1*s* of $(CH_3)_2CO$. (d) O 1*s* of CO. (e) O 1*s* of H_2CO; (f) O 1*s* of $(CH_3)_2CO_3$. Calculations done by the DFT-TP (half-core hole) and HF/STEX methods. The spectra are convoluted by a FHWM of 0.3 eV. Energies and oscillator strengths are given in Tables I, IV, and V. Experimental spectra from Hitchcock and Brion, published in Ref. 30.

Ref. 30). We predict C 1*s* and O 1*s* spectra of acetone with three peaks, while at lower resolution only two Rydberg peaks (below the IP) have been obtained from experiment.[30] Except for the main peak, all peaks have pσ character ($2p$, $3p$, and $4p$).[29] Some notable differences between STEX and DFT-TP methods are observed in the oxygen spectrum. The carbon spectrum is more complicated due to the superposition of the CO and CH_3 spectra.

On a high-resolution scale it is found that the STEX technique generally resolves more peaks than the DFT-TP technique. Some structure in the Rydberg (or mixed-valence Rydberg) parts are thus missing in the DFT case. The predicted peaks in this region are also shifted to somewhat higher energies than in the experimental spectra (or in the STEX spectra). On the other hand, in the STEX case the π^* level is intermingled with the higher-lying transitions, due to the aforementioned differential screening problem, and a shift of this level to its experimental value is often necessary in order to unravel the Rydberg structure completely;[29] in the DFT-TP calculations the relaxation of the π^* is there in the first place.

Like many other molecules the carbonyl molecules show features in the near continuum of the experimental spectra that are associated to multiple excitations, something that

requires an explicitly correlated description,[40] beyond the capability of both the DFT-TP and STEX methods. It seems that the DFT-TP method predicts too small excitation energies for the shape resonance, while the STEX method gives somewhat too large energies. In the former case this might be rationalized by too shallow a potential associated with the poor asymptotic behavior of available density functionals, while in the STEX case it probably reflects the missing screening energy for a level with valence character, here σ^*.

3. Acetylene, ethylene, and ethane spectra

The ethylene molecule has been a prototype for NEXAFS measurements in both gaseous and chemisorbed phases.[1,35] The high-resolution spectrum of free ethylene shows three distinct bands (assigned as $1b_{2g}$, $4a_g$, and $2b_{2u}$ in the molecular-orbital picture) all with anomalous internal fine structures. For the first band, C $1s$-π^*, this structure has been interpreted in terms of vibronic coupling mechanisms.[36] The spectrum has furthermore been analyzed by MS$X\alpha$,[1] by various Green's-function techniques,[36,37] and by the static exchange method.[38,39] The STEX and Green's-function energies reproduce the three-peak feature quite well. Acetylene also shows prominent C═C π^* and C—H σ features, being more dominated by the former. Ethane, being a saturated system, shows only a weak $3p$-like discrete spectrum. As for the carbonyls the π^* transition is well reproduced by the DFT-TP calculations, while the higher transitions are somewhat displaced upwards in energy; see Fig. 3. The comparison with the STEX technique indicates a general enhancement of the near-edge structures, otherwise such a comparison is not unfavorable.

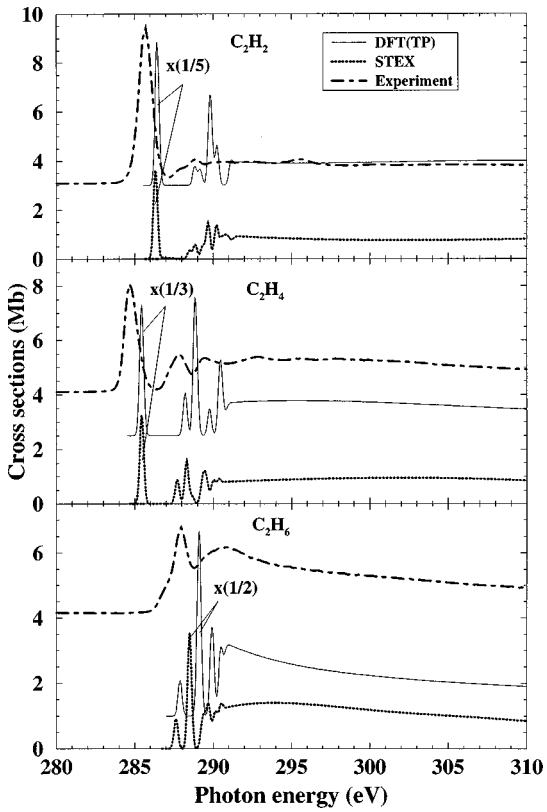

FIG. 3. C_{1s} NEXAFS spectra of hydrocarbons computed from the DFT-TP and HF/STEX (screened π^* values) methods. The calculated spectra are convoluted by a FHWM of 0.3 eV. Energies and oscillator strengths are given in Tables I and IV. Experimental values inserted on top are from C_2H_2 (Ref. 60), C_2H_4 (Ref. 61), and C_2H_6 (Ref. 62).

B. NEXAFS applications to chemisorption

There are several salient features of NEXAFS applied to the surface adsorbate systems with respect to the free species, and which are of relevance for simulations; a reduction of π^* intensity, a broadening of this band, a compression of the discrete features, and a displacement of the σ^* shape resonance toward lower energies. In a simple view the prepopulation of the π^* orbital by the surface is a possible source for the reduction of the π^* intensity, which, if so, would give a fingerprint of the catalyzing action of the particular surface. However, final-state delocalization can also serve as a means of this reduction, i.e., that the π^* orbital as populated by the excitation delocalizes from the adsorbate over the surface. The calculation of this intensity reduction has for several reasons been difficult and is of relevance for test with the DFT (and DFT-TP) approaches.

The levels with intensive absorption bind to the surface and are therefore ''self-screening,'' meaning that for these levels screening and population by excitation become simultaneous processes which to some extent calls for a treatment including electron correlation. Unlike propagator methods, in potential methods a static potential must be chosen before the spectrum is computed, and this choice might then bias the outcome. For instance, ignoring first the ''excitation'' step assuming a bare $N-1$ core hole potential, one can expect that such a procedure overestimates the screening in the potential step, and therefore that it also overestimates the diffuseness (and underestimates the intensity) of the self-screening valence level in the following excitation step. (In propagator-oriented approaches the screening, i.e., the simultaneous excitation and charge transfer, is accommodated; such methods are, however, not yet scalable for larger species in the NEXAFS case). The current DFT method is a potential method in that the spectrum is obtained from the set of eigenpairs of a diagonalization of a potential. However, it is also relevant to explore the concept of a *transition* state potential since it might avoid some of the overscreening associated with $N-1$ potentials.

The amount of screening is also dependent on the correct charge distribution in the initial state. The positioning of the metallic bands (e.g., the $3d$ bands for first-row transition metals) with respect to the adsorbate orbital levels can be crucial in this respect, and here DFT gives a substantially improved description of adsorption on metals than do Hartree-Fock-based techniques [see N/Cu(100), below]. A third aspect to consider is evidently the cluster dependence of the charge distribution and the spectral features. For chemisorbed carbonyls the charge transfer through the strong acceptor π^* bond is balanced by adsorbate to metal donation through the carbon 5σ bond, and this balance can be delicately dependent on the choice of cluster and inclusion of dynamical correlation.

1. NEXAFS of the N/Cu_{61} *cluster*

The chemisorption properties of first-row atoms on metal surfaces has been of theoretical interest for calibration of

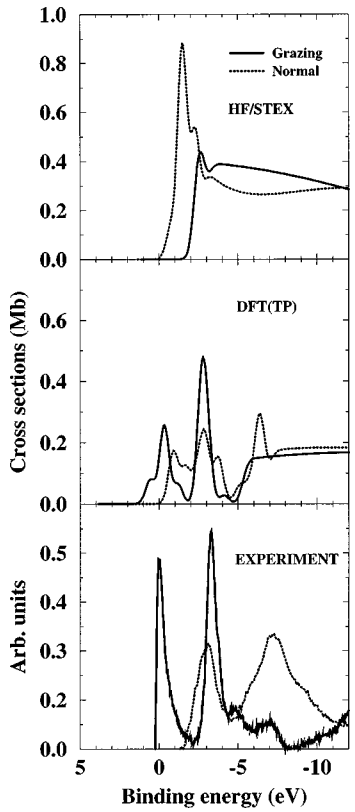

FIG. 4. Computed N_{1s} NEXAFS spectra for N/Cu_{61} using the HF-STEX and DFT-TP methods compared with experiment from Refs. 41, 42, and 63.

different approaches to chemisorption, and to investigate the degree of $3d$ involvement in the bonding. In the particular case of N/Cu(100) we recently investigated the contribution to the binding energy from dynamical correlation involving the $3d$ shell, and found very large contributions; the difference between a simple valence correlation scheme using Hartree-Fock and the modified coupled pair functional correlation method with $3d$ correlation included was of the order of 60 kcal/mole.[27] This energetic effect was accurately given within the gradient-corrected DFT framework and we have followed up on this success by computing NEXAFS and XES spectra for N/Cu(100).[28] Since this provides a particularly illustrative example of the strength of the DFT approach when dynamical correlation must be included, we will briefly discuss the results for the largest Cu_{61} cluster model here.

The spectra computed using both the HF-STEX and DFT-TP approaches are compared with the experimental $N(1s)$ spectrum[41,42] in Fig. 4. The experiment shows a very pronounced two-peak structure both in normal and grazing incidences. In grazing incidence, measuring the p_z character around the nitrogen, the peaks are particularly sharp and appear at a somewhat lower energy than in the spectrum taken at normal incidence ($p_{x,y}$), which furthermore shows much broader structures. Both the grazing and normal spectra are very well reproduced by the DFT-TP approach, but the HF-STEX approach completely fails to reproduce even the qualitative aspects of the orbital structure. This is due to the strong interaction with the $3d$ shells and covalent bond formation between N $2p$ and Cu $3d$; in a theoretical treatment this requires dynamical correlation to be included to compensate for the loss of exchange interaction within the strongly coupled $3d$ shell. Already from the correlation contribution to the chemisorption energy it is clear that the Hartree-Fock picture leaves out main components of the bonding, but these are very well recapitulated by the DFT-TP approach, including the changes to the unoccupied molecular orbitals, as evidenced from the computed spectra.

2. NEXAFS of the CO/Cu_{50} *cluster*

Figure 5 shows the results of simulations of the C $1s$ and O $1s$ NEXAFS spectra of CO/Cu_{50} modeling on-top chemisorption of CO on Cu(100). The chemisorption geometry has been optimized at the DFT level using gradient-corrected functionals for an all-electron CO/Cu_{14} cluster. The distance between the carbon atom and the top plane of Cu atoms was determined to be $3.79a_o$, $0.20a_o$ larger than the experimental value of $3.59a_o$,[43] while the optimized CO distance was $0.01a_o$ shorter than the experimental value of $2.19a_o$.

We find that large clusters must be considered in order to obtain a significant intensity reduction of the π^* intensities, something that complies with that the computed chemisorption energy for the Cu_{14} cluster only accounts for about half (8 kcal/mole) of the full chemisorption energy (16 kcal/mole) obtained from the CO/Cu_{50} cluster.[43] For the intensity the CO/Cu_{50} cluster gives a reduction compared to the gas phase by roughly a factor of 2 for both C $1s$-π^* and O $1s$-π^* transitions (more precisely a reduction to 47% and 55% of the respective gas-phase intensities). It is relevant here to compare with the corresponding finding with HF-STEX calculations using an $N-1$ potential on the same model, which gave an eightfold decrease of the C $1s$-π^* and a 6.6-fold decrease of the O $1s$-π^* intensity going from CO to CO/Cu_{50}, i.e., a significantly enhanced reduction. This was traced mostly to an overscreening of the $N-1$ core hole state through charge-transfer into the $p\pi^*$ level. The experiment gives a more moderate reduction; to 40% and 60% of the gas-phase C $1s$-π^* and O $1s$-π^* intensities, respectively (converted oscillator strengths).[44] The improved agreement with experiment given here by the DFT-TP intensities is notable, but requires thus a large cluster to reach. The reason for this improvement is twofold: a better description of the interaction with the copper $3d$ ''band'' and thus a better description of the charge localization in the ground state, and second, a ''better'' potential avoiding some of the overscreening. The improvement can thus be associated with both the DFT and TP parts of the DFT-TP method. We regard the transition potential as a better average choice for the screening problem, while a very accurate treatment still calls for an explicit correlation method, which evidently is beyond the scope of the present possibilities.

From the DFT-TP calculation, a great deal of the spectrum compression between the ionization potential (IP) and the core-π^* excitation energy is obtained; from a difference of 9.7 eV for free CO, to 2.3 eV for CO/Cu_{50} to about 1.5 eV experimentally.[45] The STEX values are here 8.0 and 3.3 eV (Ref. 33). It should be noted that our excitation energies are referred to the computed IP, which in the cluster model is different from the Fermi level of the infinite system. The experimental IP refers to the Fermi energy (x-ray-photoemission spectroscopy ionization limit) and is several

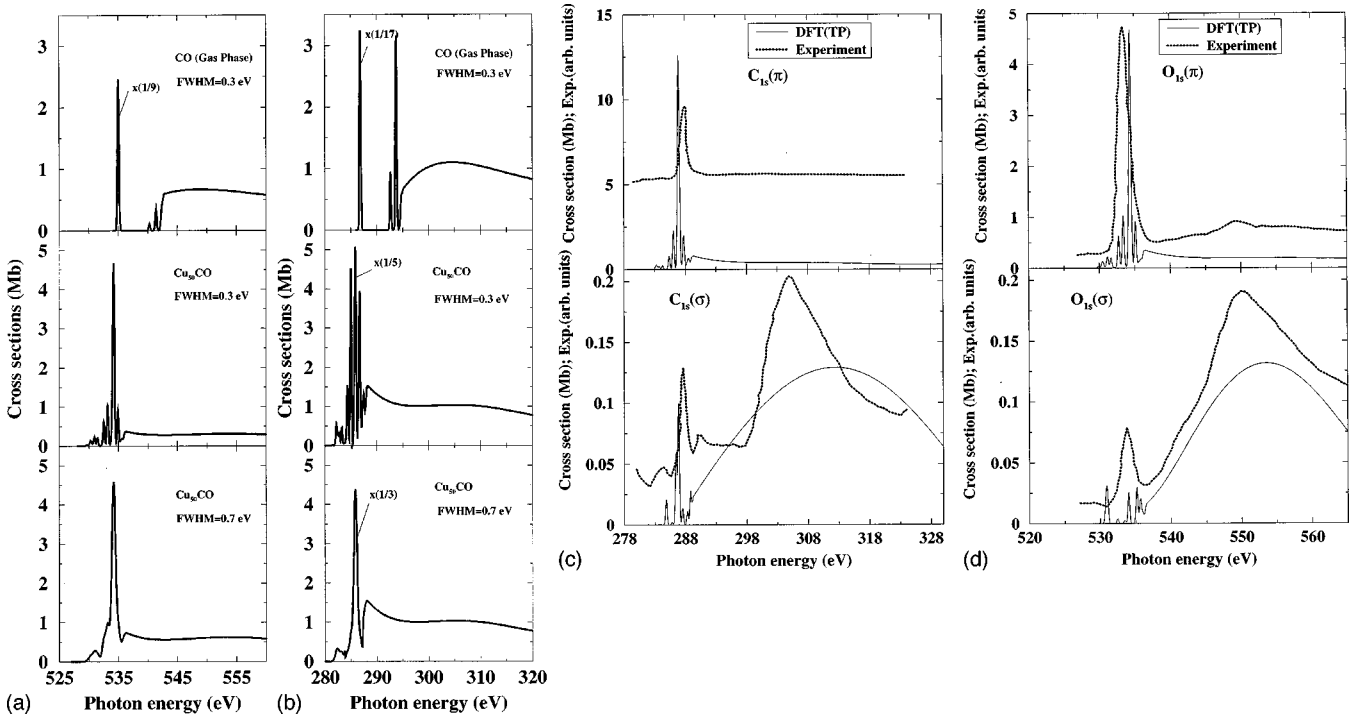

FIG. 5. (a) C_{1s} and (b) O_{1s} NEXAFS spectra of CO and CO/Cu_{50} computed from the DFT-TP method. (c) Experimental spectra obtained from Ref. 45.

eV below the computed IP for CO/Cu_{50}; however, referring to the binding energy, defined as the Fermi energy plus the work function, the CO/Cu_{50} value (292.8 eV) is fairly close to the experiment ($\simeq$291 eV).[45]

It is notable that, while the carbon π^* excitation energy slightly increases with cluster size, the corresponding oxygen excitation energy decreases. Otherwise many of the main characteristics for the O 1*s* NEXAFS spectrum are in common with those of the C 1*s* spectrum. The compression in the case of oxygen is slightly smaller than for carbon, going from 8.8 to 2.3 eV (7.0–3.1 eV are the corresponding STEX values). In the experimental spectra the free and adsorbed π^* excitation energies are the same for carbon but differ by half an eV for oxygen.[44]

The compression and the constancy of π^* transition energies can be seen as an effect of the self-shielding by the localized π^* level discussed here. The back-donation to the CO group is thus less effective for 1*s* excitation than for ionization, and the core excited state is less stabilized than the core hole leading to the compression of the spectra. The differences in the carbon and oxygen spectra might be rationalized in the different populations of the π^* level over the two sites. Much of the screening of the oxygen core takes place through the 1π orbital rather than the π^*, enhancing the carbon nature of the latter and thereby decreasing the total energy through a more effective backbonding.

In contrast to the STEX technique, for which in each case only one strongly absorbing π^* level is observed, but seemingly in agreement with observations in other metal carbonyl systems,[1] shoulders due to transitions to metal conduction states are predicted by the DFT-TP method. These are of π symmetry and have large amplitudes on the cluster. One also notes, from Fig. 6, that the C $1s$-π^* transition itself (albeit not the O $1s$-π^* transition) is split in the cluster calculations into several close-lying components, which mimic the formation of a band but which, with ordinary spectrometer convolution, would still appear as one band. The higher Rydberg states are quenched for chemisorbed systems and the above-

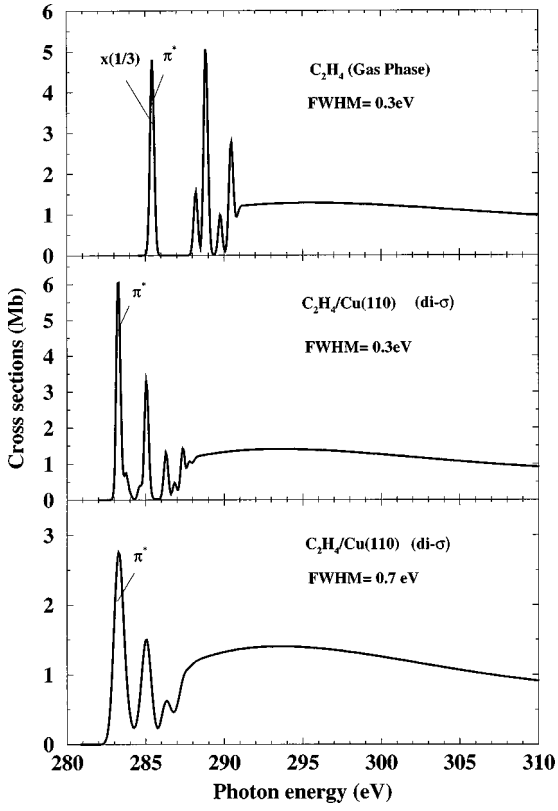

FIG. 6. C_{1s} NEXAFS spectra of C_2H_4 and $C_2H_4Cu_{50}$ computed from the DFT-TP method.

mentioned shortcomings of the long-range behavior of density functionals is of no serious consequence for the actual interpretation. On the other hand, the σ-shape resonance, which forms a ''usable'' feature clearly observable in the experiment is, however, only faintly reproduced by the DFT-TP method, something that might stem from a too shallow potential. Development of DFT/LDA theory, such as the asymptotically corrected LDA by Casida,[46] will probably be very relevant in this context.

3. Acetylene and ethylene on Cu(110)

As for carbonyls, NEXAFS has been used as an instrument to analyze the interaction of hydrocarbons with transition-metal surfaces.[35,47] The bonding has been analyzed in similar terms, i.e., with an acceptor bond between metal $d\pi$ and hydrocarbon π^* levels and a bond between the metal $p\sigma$ and hydrocarbon π levels.[48,49] In contrast to carbonyls the hydrocarbons bind side on (chains) or flat on (rings). However, the interpretation of the NEXAFS spectra of surface-adsorbed hydrocarbons has not been straightforward; calculations of free species have in some instances contradicted the results from angular-resolved surface measurements with respect to distribution of σ and π states.[50] The importance of adsorbate restructuring in this context has recently been proposed, e.g., the chemisorption-induced changes in the adsorbate structure may lead to states of symmetry that cannot be anticipated by the adsorbate in its ground-state geometry.[51] For instance, the first excited triplet state of acetylene corresponds to a $\pi \rightarrow \pi^*$ excitation, leading to a loss of bond order and a substantial (0.12 Å) elongation of the bond, and with the hydrogens bending up to a C-C-H angle that is close to 130°. Similar results are obtained for the triplet state of ethylene. These prepared triplet states of the respective molecules form good precursors for the actual optimum geometries when adsorbed to a Cu(110) surface, here considered in the di-σ form; in both cases the C-C-H angle is close to 130°, and the bond length increase is substantial, 0.11 Å for acetylene and 0.06 Å for ethylene.[51] The excitation to the triplet state thus corresponds to a rehybridization going to sp^2-hybridized carbons with a radical character; each of the carbons so being prepared for forming a covalent bond to the substrate.

In both the acetylene and ethylene x-ray-absorption spectra we predict reduction in the intensity of the π^* intensity and compression of the spectral energies, i.e., between the π^* excitation energy and the IP. The intensity reduction is of similar magnitude as found for the CO/Cu_{50} species; the C_2H_2/Cu_{14} gives a reduction to 25% and C_2H_4/Cu_{14} to 39% of the respective gas-phase intensities. The energy compressions are, however, rather small; from 5.3 to 2.9 eV for acetylene and from 5.7 to 5.0 eV for ethylene (see Fig. 7).

For acetylene and ethylene adsorbed on Cu(100) not much more than the π^* band can be discerned in the discrete spectra.[35,47] However, here, for the Cu(110) di-σ configuration, we predict a possibility to resolve at least the second discrete transition which thus lies closer to the π^* band than in the free phase, but still significantly lower than the IP's computed for the respective Cu_{50} cluster. A notable difference between the two species is the occurrence of a pre-π^* shoulder in the acetylene case, which seems similar to the one predicted for the carbon spectrum of CO/Cu_{50}, having large amplitudes on the cluster, and which might indicate transitions to ''metal conduction'' states.

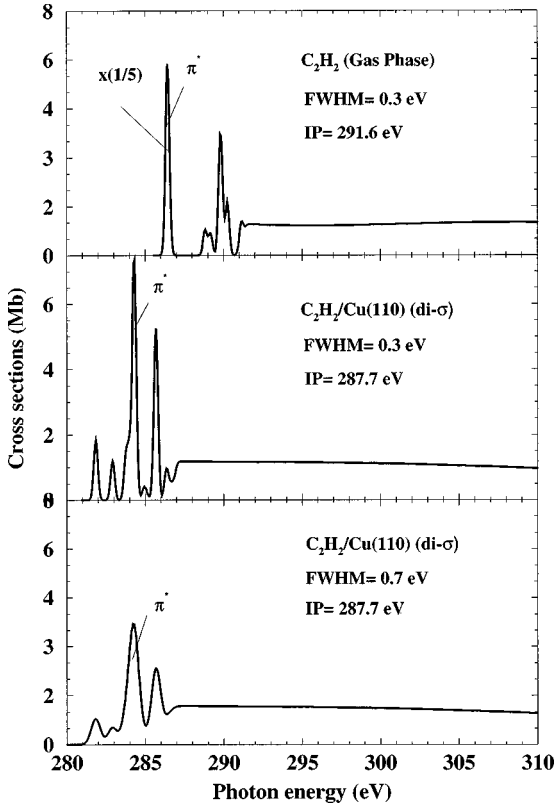

FIG. 7. C_{1s} NEXAFS spectra of C_2H_2 and $C_2H_2Cu_{50}$ computed from the DFT-TP method.

IV. CONCLUSIONS

Results from calculations of near-edge x-ray-absorption spectra using density-functional and transition-potential theory have been presented and analyzed in the present work. A number of carbonyl and hydrocarbon compounds, as well as cluster models of Cu(100) or Cu(110) with chemisorbed atomic nitrogen, CO, or unsaturated hydrocarbons, have been selected for the purpose. It is shown that calculations of this kind can reproduce the spectral profiles near the ionization threshold that now can be measured by synchrotron experiments in the x-ray region. The accuracy and the significance of the method employed, DFT-TP, was here first established for smaller carbonyls. It was found that core to π^* valence excitations are very well reproduced both concerning energies and oscillator strengths when using a transition state potential, thereby confirming results of some previous works.[7,8] The absolute and relative core ionization potentials are obtained with separate-state Kohn-Sham optimization, while the core orbital energies from the DFT-TP calculation with a half-occupied core orbital notoriously overshoot the IP by a constant amount, somewhat more than an eV, irrespective of element. A simple correction accounting for this fact put the XAS spectra on a very good energy scale. Calculations of Rydberg progressions and other near-continuum features—here made possible by implementing a double-basis-set technique—showed results of somewhat inferior quality than those obtained for the first valencelike

transition, something that was referred to the incorrect asymptotic behavior of the commonly used density functionals. However, although a push up in energy and some loss of Rydberg structure into the continuum was found, the general outcome is usable for assignments. Comparison with the HF-STEX method showed complementary advantages between the two approaches for free molecules.

The salient features of NEXAFS for surface adsorbates—as modeled by N/Cu_{61}, CO/Cu_{50}, C_2H_2/Cu_{14}, and C_2H_4/Cu_{14}—are well accounted for. In particular, the compression of the spectrum and reduction of π^* intensity, for the spectra of the CO-copper cluster, reproduced experimental findings. An intensity reduction of about 50% in the carbon and oxygen spectra was obtained for a cluster as large as CO/Cu_{50}. For clusters the DFT-TP technique seems to improve over Hartree-Fock-based spectra in a couple of aspects: first, a better balance of the screening is obtained by a transition potential in the DFT case, and thereby an intensity reduction of the π^* intensity that is more in harmony with the experiment. Furthermore, the improved positioning of the copper $3d$ band with respect to the adsorbate valence levels and inclusion of dynamical correlation from the outset gives a better charge distribution in the ground state, and allows one to describe systems where first-row transition-metal $3d$ bonding is involved [e.g., N/Cu(100)]. The latter fact is of consequence both for the optimization of the adsorbate geometry and for the outcome in terms of a simulated spectrum.

[1] J. Stöhr, *NEXAFS Spectroscopy* (Springer-Verlag, Berlin, 1992).
[2] H. Ågren, V. Carravetta, and O. Vahtras, Chem. Phys. **195**, 47 (1995).
[3] O. Plachkevytch, L. Yang, O. Vahtras, H. Ågren, and L. G. M. Petterson, Chem. Phys. **222**, 125 (1997).
[4] H. Ågren, V. Carravetta, O. Vahtras, and L. G. M. Pettersson, Theor. Chem. Acc. **97**, 14 (1997).
[5] V. Carravetta, J. Phys. B **21**, 1777 (1988).
[6] Z. Y. Wu, M. Benfatto, M. Pedio, R. Cimino, S. Mobilio, S. R. Barman, K. Maiti, and D. D. Sarma, Phys. Rev. B **56**, 228 (1997).
[7] M. Stener, A. Lisini, and P. Decleva, Chem. Phys. **191**, 141 (1995).
[8] C. H. Hu and D. P. Chong, Chem. Phys. Lett. **262**, 729 (1996).
[9] L. Triguero, L. G. M. Pettersson, and H. Ågren, J. Phys. Chem. (to be published).
[10] J. C. Slater, Adv. Quantum Chem. **6**, 1 (1972).
[11] J. C. Slater and K. H. Johnsson, Phys. Rev. B **5**, 844 (1972).
[12] D.R. Salahub, R. Fournier, P. Mlynarski, I. Papai, A. St-Amant, and J. Ushio, in *Density Functional Methods in Chemistry*, edited by J. Labanowski and J. Andzelm (Springer, New York, 1991), p. 77; A. St-Amant, Ph.D. thesis, Université de Montréal, 1992. The present version of the program was substantially modified by L. G. M. Pettersson.
[13] P. W. Langhoff, in *Electron Molecule and Photon Molecule Collisions*, edited by T. N Rescigno, B. V. McKoy, and B. Schneider (Plenum, New York, 1979), p. 183.
[14] H. Ågren, V. Carravetta, O. Vahtras, and L. G. M. Pettersson, Chem. Phys. Lett. **222**, 75 (1994).
[15] W. Kutzelnigg, U. Fleischer, and M. Shindler, *NMR-Basic Principles and Progress* (Springer-Verlag, Heidelberg, 1990), Vol. 23, p. 165.
[16] S. Huzinaga, J. Chem. Phys. **42**, 1293 (1965).
[17] J. P. Perdew and Y. Wang, Phys. Rev. B **33**, 8800 (1986).
[18] A. D. Becke, Phys. Rev. A **38**, 3098 (1988).
[19] J. P. Perdew, Phys. Rev. B **34**, 7406 (1986).
[20] J. P. Perdew, in *Electronic Structure of Solids*, edited by P. Ziesche and H. Eschrig (Akademie Verlag, Berlin, 1991).
[21] J. P. Perdew and Y. Wang, Phys. Rev. B **45**, 13 244 (1992).
[22] J. P. Perdew, J. A. Chevary, K. A. Jackson, S. H. Vosko, M. R. Pederson, D. J. Singh, and C. Fiolhais, Phys. Rev. B **46**, 6671 (1992).
[23] S. H. Vosko, L. Wilk, and M. Nusair, Can. J. Phys. **58**, 1200 (1980).
[24] A. J. H. Wachters, J. Chem. Phys. **52**, 1033 (1970).
[25] A. Mattsson, I. Panas, P. Siegbahn, U. Wahlgren, and H. Åkeby, Phys. Rev. B **36**, 7389 (1987).
[26] R. Manne, J. Chem. Phys. **52**, 5733 (1970).
[27] L. Triguero, U. Wahlgren, L. G. M. Pettersson, and P. Siegbahn, Theor. Chim. Acta **94**, 297 (1996).
[28] L. Triguero and L. G. M. Pettersson, Surf. Sci. **398**, 70 (1998).
[29] L. Yang, H. Ågren, V. Carravetta, and L. G. M. Pettersson, Phys. Scr. **54**, 614 (1996).
[30] A. P. Hitchcock and C. E. Brion, J. Electron Spectrosc. Relat. Phenom. **19**, 231 (1980).
[31] L. G. M. Pettersson, H. Ågren, B. L. Schürmann, A. Lippitz, and W. E. S. Unger, Int. J. Quantum Chem. **63**, 749 (1997).
[32] I. Kojima, A. K. Srivastava, E. Miyazaki, and H. Adachi, Chem. Phys. **84**, 867 (1986).
[33] L. G. M. Pettersson, H. Ågren, O. Vahtras, and V. Carravetta, Surf. Sci. **365**, 581 (1996).
[34] L. Yang, H. Ågren, L. G. M. Pettersson, and V. Carravetta, J. Electron Spectrosc. Relat. Phenom. **82**, 209 (1997).
[35] D. Arvantis, J. Singh, H. Rabus, T. Ledere, and K. Baberschke, Phys. Rev. B **45**, 1518 (1991).
[36] F. X. Gadea, H. Köppel, J. Schirmer, L. S. Cederbaum, K. J. Randall, A. M. Bradshaw, Y. Ma, F. Sette, and C. T. Chen, Phys. Rev. Lett. **66**, 883 (1991).
[37] C. M. Liegener and H. Ågren, Phys. Rev. B **48**, 789 (1993).
[38] J. A. Sheehy, T. J. Gil, C. L. Winstead, R. E. Farren, and P. W. Langhoff, J. Chem. Phys. **91**, 1796 (1989).
[39] V. Carravetta, H. Ågren, L. G. M. Pettersson, and O. Vahtras, J. Chem. Phys. **102**, 5589 (1995).
[40] H. Ågren and R. Arneberg, Phys. Scr. **30**, 55 (1984).
[41] T. Wiell, Ph.D. thesis, University of Uppsala, 1995.
[42] T. Wiell, J. E. Klepeis, P. Bennich, O. Björneholm, N. Wassdahl, and A. Nilsson (unpublished).
[43] A. van Dalen, Y. S. Li, J. M. Newsam, and R. A. van Santen, J. Chem. Phys. **100**, 2279 (1996).
[44] A. Nilsson and N. Mårtensson, Physica B **208**, 19 (1995).
[45] O. Björneholm, A. Nilsson, E. O. F. Zdansky, A. Sandell, H. Tillborg, J. N. Andersen, and N. Mårtensson, Phys. Rev. B **47**, 2308 (1993).
[46] M. E. Casida (private communication).

[47] H. Rabus, D. Arvantis, M. Domke, and K. Baberschke, J. Chem. Phys. **96**, 1560 (1992).
[48] M. J. S. Dewar, Bull. Soc. Chim. Fr. **18**, C79 (1951).
[49] J. Chatt and L. A. Duncanson, J. Chem. Soc. **1953**, 2939.
[50] C. M. Liegener and H. Ågren, J. Chem. Phys. **99**, 2821 (1993).
[51] L. Triguero, L. G. M. Pettersson, B. Minaev, and H. Ågren, J. Chem. Phys. **108**, 1193 (1998).
[52] R. N. S. Sodhi and C. E. Brion, J. Am. Chem. Soc. **111**, 5051 (1985).
[53] R. McLaren, S. A. C. Clark, I. Ishii, and A. P. Hitchcock, Phys. Rev. A **26**, 1683 (1987).
[54] R. B. Kay, Ph. E. van der Leeuw, and M. J. van der Wiel, J. Phys. B **10**, 2513 (1977).
[55] M. B. Robin, I. Ishii, R. McLaren, and A. P. Hitchcock, J. Electron Spectrosc. Relat. Phenom. **47**, 53 (1988).
[56] T. K. Sham, B. X. Yang, J. Kirz, and J. S. Tse, Phys. Rev. A **40**,652 (1989).
[57] A. Hitchcock, M. Weinelt, A. Nilsson, and J. Stöhr (unpublished).
[58] A. Barth and J. Schirmer, J. Phys. B **18**, 867 (1985).
[59] M. Domke, C. Xue, A. Puschmann, T. Mandel, E. Hudson, D. A. Shirely, and G. Kaindl, Chem. Phys. Lett. **173**, 122 (1990).
[60] A. P. Hitchcock and C. E. Brion, J. Electron Spectrosc. Relat. Phenom. **10**, 317 (1977).
[61] R. McLaren, S. A. Clark, I. Ishii, and A. P. Hitchcock, Phys. Rev. A **36**, 1683 (1987).
[62] I. Ishii, R. McLaren, A. P. Hitchcock, K. D. Jordan, H. Choi, and M. B. Robin, Can. J. Chem. **66**, 2104 (1988).
[63] T. Wiell, A. Nilsson, N. Wassdahl, P. Bennich, N. Mårtensson, J. Nordgren, O. Björneholm, and J. Stöhr (unpublished).